Research in Astronomy and Astrophysics, 23:095028 (11pp), 2023 September https://doi.org/10.1088/1674-4527/ace90f

The Tianlin Mission: A 6 m UV/Opt/IR Space Telescope to Explore Habitable Worlds and the Universe

Wei Wang[1], Meng Zhai[2], Gang Zhao[1,3], Shen Wang[1], Jifeng Liu[1], Jin Chang[1], Xuejun Zhang[4], Jihong Dong[4], Boqian Xu[4], and Frank Grupp[5,6]

[1] CAS Key Laboratory of Optical Astronomy, National Astronomical Observatories, Chinese Academy of Sciences, Beijing 100101, China; wangw@nao.cas.cn
[2] CAS South America Center for Astronomy, National Astronomical Observatories, Chinese Academy of Sciences, Beijing 100101, China; mzhai@nao.cas.cn
[3] University of Chinese Academy of Sciences, Beijing 100049, China
[4] The Changchun Institute of Optics, Fine Mechanics and Physics, Chinese Academy of Sciences, Changchun 130033, China
[5] Universitäts Sternwarte München, Scheinerstr 1, München D-81679, Germany
[6] Max Planck Institute for Extraterrestrial Physics, Giessenbachstrasse 1, D-85748 Garching, Germany
Received 2022 February 7; revised 2023 June 17; accepted 2023 July 14; published 2023 September 6

Abstract

It is expected that ongoing and future space-borne planet survey missions including Transiting Exoplanet Survey Satellite (TESS), PLATO and Earth 2.0 will detect thousands of small to medium-sized planets via the transit technique, including over a hundred habitable terrestrial rocky planets. To conduct a detailed study of these terrestrial planets, particularly the cool ones with wide orbits, the exoplanet community has proposed various follow-up missions. The currently proposed European Space Agency mission Ariel is the first step for this purpose, and it is capable of characterization of planets down to warm super-Earths mainly using transmission spectroscopy. The NASA Large Ultraviolet/Optical/Infrared Surveyor mission proposed in the Astro2020 Decadal Survey white paper will endeavor to further identify habitable rocky planets, and is expected to launch around 2045. In the meanwhile, China is funding a concept study of a 6 m class space telescope named Tianlin (a UV/Opt/NIR large aperture space telescope) that aims to start its operation within the next 10–15 yr and last for 5+ yr. Tianlin will be primarily aimed at the discovery and characterization of rocky planets in the habitable zones around nearby stars and to search for potential biosignatures mainly using the direct imaging method. Transmission and emission spectroscopy at moderate to high resolution will be carried out as well on a population of exoplanets to strengthen the understanding of the formation and evolution of exoplanets. It will also be utilized to perform in-depth studies of the cosmic web and early galaxies, and constrain the nature of dark matter and dark energy. We describe briefly the primary scientific motivations and main technical considerations based on our preliminary simulation results. We find that a monolithic off-axis space telescope with primary mirror diameter larger than 6 m equipped with a high contrast coronagraph can identify water in the atmosphere of a habitable-zone Earth-like planet around a Sun-like star. More simulations for the detectability of other key biosignatures including O_3, O_2, CH_4 and chlorophyll are coming.

Key words: space vehicles – Planetary Systems – astrobiology – planets and satellites: terrestrial planets – instrumentation: high angular resolution – instrumentation: spectrographs

1. Introduction

The first extrasolar planet (exoplanet) orbiting a solar-type star was discovered in 1995 (Mayor & Queloz 1995) via the radial velocity (RV) method. This technique endeavors to measure precisely the periodic RV variation of a star, with the RV amplitude varying from about 100 m s^{-1} for Jupiter-like planets to a few m s^{-1} for Earth-like planets around M type stars. Since then, 5084 exoplanets have been detected and confirmed,[7] among which most were discovered via the RV and transit methods. While the RV technique was the most efficient method available before 2009, the transit method, which attempts to detect planets by searching for small dimming in the light curve when a planet transits and blocks a small portion of its host star's disk, has turned out to be much more efficient in revealing planet candidates. The Kepler mission (Borucki et al. 2011) and the K2 mission (Howell et al. 2014) have opened a new era with thousands of exoplanets detected in less than 10 yr, contributing a lot of new knowledge on exoplanets, particularly related to small and rocky planets.

The Transiting Exoplanet Survey Satellite (TESS) project (Ricker et al. 2015) has been monitoring approximately 200,000 stars brighter than 12 mag in *V*, and it is expected to discover more than 14,350 planets including over 2100 planets

[7] https://exoplanetarchive.ipac.caltech.edu/index.html accessed on 2022 September 5.

smaller than $4R_{\oplus}$ and 280 smaller than $2R_{\oplus}$. About 70 habitable zone (HZ) planets will be detected but should be mostly orbiting M dwarfs (Barclay et al. 2018). As of 2020 September, TESS finished its primary mission, with 2174 candidate planets and 67 confirmed planets reported. It was recently approved to continue working until 2022 and should find more planets than the original predictions. The PLAnetary Transits and Oscillations of stars (PLATO) space mission (Rauer et al. 2014) is expected to be launched in 2026, which will take a further step to search for small and cool planets. It will stare at two 2232 $\deg^2$ sky areas for 2–3 yr, aiming to detect terrestrial exoplanets at orbits up to the HZs of solar-type stars with magnitude between 4 and 16 mag (Rauer et al. 2014). It will observe up to 1 million stars, and may detect 13,000 planets, including 2000 planets smaller than $2R_{\oplus}$, and 6–280 of them in HZs. A new survey mission named Earth 2.0 (or ET for short) has been recently proposed in China, which aims to detect a dozen Earth-like planets around solar-type stars, and thousands of other types of planets from sub-Earths to Jupiters. ET is planned to launch in 2026 and operate for 4 yr or more (Ge et al. 2022). In addition to the above-mentioned transit survey missions, a space-borne astrometric mission named Closeby Habitable Exoplanet Survey (CHES) was proposed for the detection of habitable planets of nearby solar-type stars (Ji et al. 2022).

Therefore, various missions in the 2020s may discover thousands of rocky planets orbiting stars that are bright enough for ground-based RV follow-up confirmations, including tens or hundreds of temperate terrestrial planets with liquid water pooling on their surfaces. Only very few of the systems, with nearby cool host stars, relatively large planet radii and short orbital periods, have been preliminarily investigated by currently available telescopes (Benneke et al. 2019; Swain et al. 2021), but most of them have to wait for future missions for atmospheric characterization.

The Atmospheric Remote-sensing Infrared Exoplanet Large-survey (Ariel) mission (Tinetti et al. 2016) has been selected by the European Space Agency (ESA) as the fourth medium-class mission, and is scheduled for launch in 2029. The goal of the Ariel mission is to obtain spectra of $\sim$1000 known planets orbiting nearby stars using the transit method, to study and characterize the planets' chemical compositions and thermal structures, in order to address the fundamental questions of how planetary systems form and evolve. Ariel will mainly focus on gaseous and rocky planets with equilibrium temperatures higher than 500 K. Given its meter-class aperture, it is not capable of investigating the atmospheres of habitable terrestrial planets around GK type stars, unfortunately.

One of the key scientific objectives of the James Webb Space Telescope (JWST; Gardner et al. 2006) is to determine the physical and chemical properties of planetary systems, and investigate the potential for the origins of life in those systems. However, there is no spectrograph equipped behind its coronagraph, which means it does not provide the capability of obtaining planet spectra directly, and transit spectroscopy at low-to-intermediate resolution (i.e., $R = 150$–4000) is the only technique to obtain spectra of exoplanets by JWST. In this case, terrestrial planets in the HZs of FGK stars more than 3 pc away could barely be investigated in less than 100 hr, simply because the star-to-planet photon ratio is overwhelming large which makes it almost hopeless to acquire enough signal-to-noise ratio (S/N) for planet spectra in its mission lifetime. However, there is a lack of HZ terrestrial planets around nearby FGK stars that cannot be made up for in the near future.

The 2.4 m Nancy Grace Roman Space Telescope (or RST for short) is NASA's next flagship observatory, planned to launch no later than 2027. The Coronagraph Instrument (CGI) on RST will be the first space coronagraph that aims to demonstrate high-contrast technology necessary for exoplanet imaging and spectroscopy. The predicted contrast ratio of CGI is below 10^{-8} and close to 10^{-9}, and thus is about 2–3 orders of magnitude better than any current facility, and should allow direct imaging and spectroscopy of hot to cold Jupiters (Kasdin et al. 2020).

The CGI's on board experience within this decade should shed crucial light on future larger missions, including Habitable Exoplanet Observatory (HabEx; Gaudi et al. 2020), and Large Ultraviolet/Optical/Infrared Surveyor (LUVOIR; The LUVOIR Team 2019). An intermediate mission of these two is prioritized in the Astro2020 Decadal Survey and is to be designed in the coming years and launched in the first half of the 2040s. It would subsequently provide opportunities to discover and characterize habitable Earth-like planets if the mission develops smoothly.

The next generation of large ground-based telescopes, including the Thirty Meter Telescope (TMT), Extremely Large Telescope (ELT) and the Giant Magellan Telescope (GMT), are expected to have their first light in 2027 or later. High-contrast coronagraphic instruments aided with extreme adaptive optics (ExAO) systems could be built and operating by 2035, and they could help to characterize spectrally warm giant planets with a contrast ratio of $\sim 10^{-8}$. It is worth noting that high-dispersion spectroscopy (Snellen et al. 2014), when combined with high-contrast imaging, i.e., HCI+HDS, using advanced coronagraphs on large telescopes, may allow atmospheric studies of a small sample of habitable-zone Earth-like planets around nearby red dwarfs (Snellen et al. 2015; Wang et al. 2017).

To conclude, there is currently no approved or planned mission before the 2040s that will be able to characterize the atmospheres of temperate rocky planets around GK stars. Foreseeing the lack of the key capability to detect and identify extraterrestrial biosignatures within the next decade, the Chinese Academy of Sciences (CAS) has been funding a concept study for a 6 m space telescope named Tianlin since

2019, aiming to characterize habitable planets around nearby GK type stars (Wang et al. 2020).

This paper is organized as follows. We present in Section 2 an overall introduction to Tianlin and its main science objectives. Section 3 summarizes the currently known potential biosignatures and our target molecular species, and introduces the model and methods that we adopt for simulation. Constraints on technical requirements based on our simulation are presented and discussed in Section 4, followed by a brief summary in Section 5.

2. Tianlin and its Scientific Objectives

The Tianlin mission is a proposed space telescope with an aperture size of 4–6 m launched to the Sun–Earth L2 point (SEL2) halo orbit. Its primary objective is the characterization of rocky planets, particularly HZ terrestrial planets around nearby G and K type stars. The telescope is designed to be an off-axis 3-mirror system with a primary mirror of 4–6 m, including four Fine Guiding Sensors to aid in high accuracy and high stability line-of-sight pointing, an advanced coronagraph and one backend spectrograph with resolution varying from ~100 to 15,000. The main techniques to be used include direct spectroscopy via the coronagraph and transit spectroscopy with a low to high resolution spectrograph, covering a full range from the ultraviolet (UV) to near-infrared (NIR, 0.20–1.7 μm). Like the similar missions including HabEx and LUVOIR, the SEL2 quasi-halo orbit is considered for Tianlin, for the consideration of a stable dynamical, thermal environment and the capability of continuous staring for tens to hundreds of hr. This orbit can be reached by a Chinese Long March 5 rocket, and was visited once by the Chinese Chang'e-2 mission in 2012.

Tianlin is different from HabEx in several aspects. First, the aperture size of Tianlin may be as large as 6 m. Second, Tianlin will be equipped with a high-resolution spectrograph to conduct high-resolution spectroscopic atmospheric studies and enable the HCI+HDI technique to better trace spectral signals, while HabEx will not. Lastly, a formation-fly starshade configuration is not considered for Tianlin at the current stage. The NASA IROUV mission is a hybrid of HabEx and LUVOIR named Habitable Worlds Observatory (HWO), and it aims to directly image planets including Earth-like exoplanets around Sun-like stars and characterize their atmospheres. This mission is planned to be developed in the next 5 yr, and could be launched in the first half of the 2040s.

The mission has a primary science objective to search for and characterize the atmospheres of nearby exoplanets, particularly Earth-like planets and close-in rocky planets around G and K stars, to explore their habitability, and to search for potential biosignatures in their atmospheres or on their surfaces. We define in this work an Earth-like planet as a rocky planet with a radius between 0.6 and 1.4$R_\oplus$ orbiting around a G or K-type star within the respective conservative HZs following the work by Kopparapu et al. (2014). We define a twin Earth as a rocky planet with a radius of 1$R_\oplus$ orbiting a G2 star at 1 au. A close-in rocky planet in our sample is a planet that orbits a G or K dwarf star between the inner limits of the conservative and optimistic HZs. It may also be habitable, and should be easier for atmospheric characterization compared to Earth-like and Earth-twin planets.

The detailed target sample for this objective is to be compiled in the following years, based on transit and direct imaging surveys of nearby stars. It will consist not only of transiting planets but also of non-transiting planets. As summarized in Section 1, there will be plenty of transiting Earth-like planets to be found by the above-mentioned transit surveys, for which Tianlin could only obtain their transmission or reflection/emission spectra during their primary/secondary transits without blocking the central stars' light. However, as will be emphasized in Section 4, such a technique may need an aperture size $D > 6$ m for detection of a molecular signal in a twin Earth orbiting a GK star brighter than $V = 5$, which has never been reported yet and is expected to be very rare. In the meantime we initiate a CubeSat mission named Nearby Earth Twin Hunter (NETH) (Wang et al. 2023, in preparation) to monitor several nearby bright GK stars with known transiting planets and to search for twin Earths, which may find the first nearby twin Earths and provide targets for the Tianlin mission.

On the other hand, obtaining planetary spectra directly and detecting molecular signals seem to be more feasible because starlight could have been extremely suppressed by next-generation advanced coronagraphs or an external starshade. Moreover, one would expect that the sample size of non-transiting twin Earths will become much larger than that of transiting ones in the future with the onset of CHES, Tianlin and other direct imaging surveys, given that statistically non-transiting planets are more abundant than transiting planets.

The secondary science goal is to obtain a comprehensive understanding of various types of planets and planetary systems, what they are made of, how they form and evolve, and what are the characteristics of their atmospheres, by conducting an in-depth spectroscopic survey of a sample (>100) of nearby rocky and gas planets with unprecedented precision and accuracy. This survey will eventually lead to a revolution in our knowledge of planetary science. The corresponding sample sizes of HabEX, and LUVOIR-A and -B are 150, 648 and 576, respectively (The LUVOIR Team 2019; Gaudi et al. 2020).

Nevertheless, Tianlin will provide key capabilities for other high-impact general astrophysical questions. For example, its high sensitivity and spatial resolution in all bands, particularly the UV bands, will help to constrain the nature of dark matter and dark energy, understand the complexity inherent in the formation and evolution of the cosmic web and galaxies, and

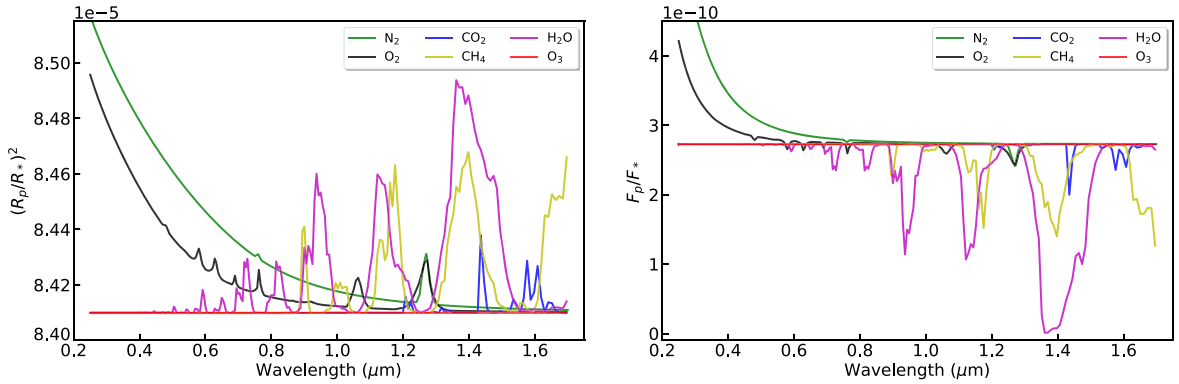

Figure 1. The model-predicted reflection (left) and transmission (right) spectra from 0.25 to 1.7 μm at $R = 150$ for N_2, CO_2, H_2O, O_2, CH_4 and O_3, drawn with differently colored lines respectively.

facilitate an in-depth examination of the connection between structures, dark matter, radiation and baryons.

The goal of exploring the habitability and detecting potential biosignatures of nearby twin Earths is extremely challenging, simply because an Earth-like object is extremely faint and is deeply embedded in its host star's light. These facts put strong constraints on the baseline setup of Tianlin, particularly its aperture size, noise level and contrast level of the starlight suppression technique, as indicated by our simulations carried out in Section 3. In the remaining part of this manuscript, we will mainly discuss the implications obtained from the first scientific objective, i.e., the search for biosignatures from exoplanets.

3. Model Description and Methodology

In this section, we describe briefly what molecules should be searched for, how we generate planet and star spectra, how to simulate observations, and estimate the required integration time for each configuration. More details will be presented in Zhai et al. (2023) (submitted).

The fundamental question we attempt to address here is whether the proposed Tianlin mission concept has the capability in its lifetime to detect a potential biosignature and habitability markers, and derive optimized mission requirements to achieve this goal. The two techniques that we consider employing are transmission spectroscopy (hereafter TMS) and HCI aided by a coronagraph.

The key signals that may provide evidence for the presence of life include gas molecules in an exoplanet atmosphere such as oxygen (O_2), ozone (O_3), methane (CH_4), nitrous oxide (N_2O) and methyl chloride (CH_3Cl), and substances on the surface, for example the vegetation "red edge" (VRE) and halophile salt. Among them, O_2, O_3 and CH_4 are our primary target species to detect and study. In addition, water (H_2O) is one of the key species required for life and its absence may be regarded as an anti-biosignature. Plenty of spectral features from these four molecules are detectable in the atmospheres of rocky planets from the near-UV (NUV) to infrared (IR) (Des Marais et al. 2002; Kiang et al. 2018; Léger et al. 2019). We also show respectively in Figures 1 and 3 the model-predicted emission and transmission spectra from individual species, and the theoretical spectrum of a twin Earth (black curve) between 0.25 and 1.7 μm at a resolution R of 150, 1000 and 15,000 (the top, middle and bottom panels of Figure 3 respectively), together with the simulated transmission and emission spectrum (left and right panels) for the $R = 150$ case.

As the first step, the simulation performed in this work is only on the detectability of H_2O in the HZ of Earth-like planets around GK stars using both direct spectroscopy and transmission spectroscopy. This is because this molecule is required for life, and is the easiest one to detect in the optical and NIR. Detecting the crucial biosignature gas O_2 is harder than H_2O, and can be achieved simply by increasing integration time in most cases. The key technical parameters used in the simulation are presented in Table 1.

Table 1
Input Parameters of the Simulation, and the Recommended Values Suggested by Our Simulation

Telescope/Instrument	Parameter Space	Recommended Value
Telescope aperture D (m)	[4, 12]	6
Detector dark current d (e^-/hr/pixel)	[0.02, 2]	0.2
Contrast level C	[10^{-11}, 10^{-7}]	10^{-10}
Throughput of spectrograph η_{spe} (%)	[40, 70]	70
Throughput of coronagraph η_{cor} (%)	[5, 20]	10
Lifetime (yr)	[5, 10]	10
Exposure time T (hr)	100–10,000	
Wavelength λ (μm)	fixed, 0.8–1.05	

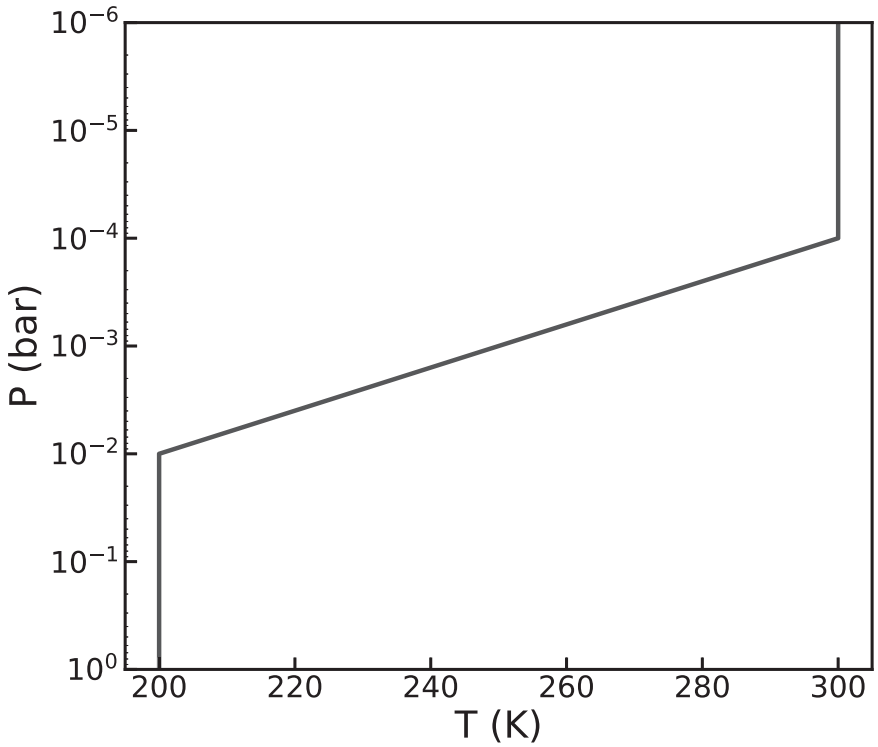

Figure 2. The T-P profile that we employ for the generation of planet spectra.

3.1. Planet Spectra Model

In this work, the reflection and transmission spectra of Earth-like planets are generated using the public code petitRADTRANS (Mollière et al. 2019), assuming an Earth-like surface and atmosphere. The temperature–pressure (T-P) profile we adopted is a simplified toy model with a thermal inversion layer included, as illustrated in Figure 2. A model atmosphere includes molecules of oxygen (O_2), ozone (O_3), methane (CH_4), water (H_2O), nitrogen (N_2) and carbon dioxide (CO_2), with their volume mixing ratios (VMRs) the same as those of Earth (listed in Table 2). Absorption, emission and scattering due to H_2O, O_2, O_3, CH_4, CO_2 and N_2 are taken into account. Their model-predicted emission and transmission spectral signatures are displayed in Figure 1.

The abundance of each molecule in petitRADTRANS is in the unit of mass fractions, which is converted to VMR utilizing the following formula

$$X_i = \frac{\mu_i}{\mu} n_i, \tag{1}$$

where X_i is the mass fraction of species i, μ_i is the mass of the molecule i, μ is 28.7, the atmospheric mean molecular weight of Earth, and n_i is the VMR of species i.

In total, $4 \times 2 \times 3 \times 2 = 48$ sets of high-resolution transmission and reflection spectra of rocky planets within HZs are generated, considering four types of host stars (G2, G8, K2, K7, see, Table 3), two types of planets ($1R_\oplus$ and $2R_\oplus$) with the same bulk compositions and three atmospheric H_2O mixing ratios of 0.1, 1 and 10 times the terrestrial value (i.e., dry, standard and wet, respectively), with or without water clouds. We note that a $2R_\oplus$ planet may have a different atmospheric composition than the Earth's, which will be amended in the

Table 2
VMRs of the Molecules Considered in the Planet Atmospheric Models

Molecular	VMR	Molecular	VMR	Molecular	VMR
O_2	0.21	O_3	10^{-7}	CH_4	0.0001
H_2O	10^{-2}, 10^{-3}, 10^{-4}	N_2	0.78	CO_2	0.0004

Table 3
Input Parameters of Planet Host Stars

Star Type	Temperature (K)	Mass ($M_\odot$)	Radius ($R_\odot$)	Semimajor Axis (au)
G2	5778	1	1	1
G8	5375	0.78	0.86	0.71
K2	4925	0.69	0.64	0.5
K7	4017	0.63	0.6	0.3

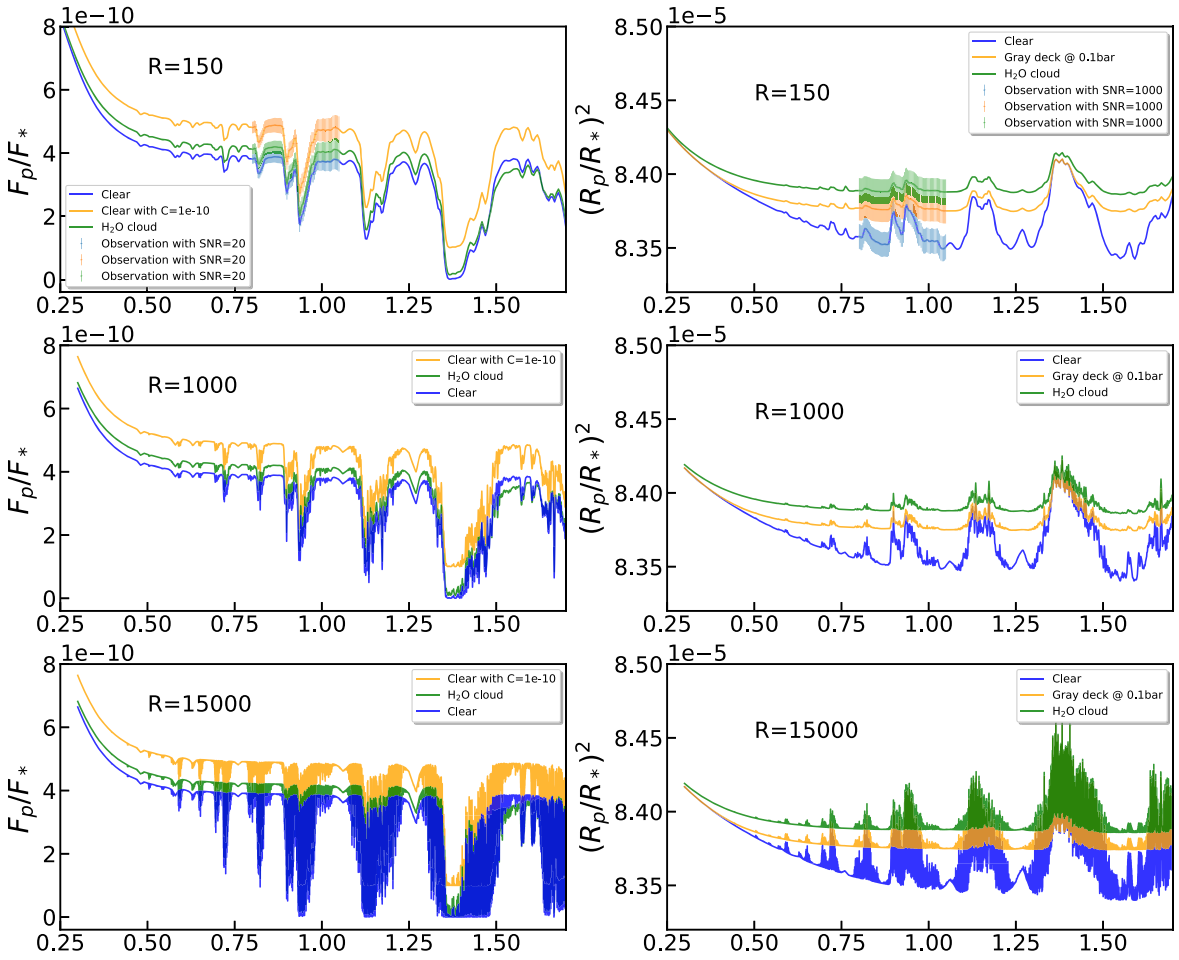

Figure 3. The simulated noise-free reflection (left) and transmission (right) spectra of an Earth twin in the NUV, optical and NIR bands of $R = 150$ (top), 1000 (middle) and 15,000 (bottom), respectively. Absorption, emission and scattering due to H_2O, O_2, O_3, CH_4, CO_2 and N_2 are taken into account. For the emission spectra, three different cases assuming cloudy or clear and different albedos are considered. For the transmission spectra, two cases assuming cloudy or clear are included. In the top two panels, spectra with S/N (0.88 μm) of 20 are overplotted for comparison. The definition of S/N is provided in Section 3.2.

future when more knowledge about such planet is obtained. The semimajor axis values tabulated in Table 3 are the conservative inner limits of HZs corresponding to each spectral type following the work by Kopparapu et al. (2014) for G8 to K7 dwarf stars, and are exactly the Earth's semimajor axis for a G2 dwarf.

For water clouds, the irregular shapes of water clouds as condensates in the atmosphere are included, with a mean particle size of 25 μm. For transmission spectra, we also calculate the spectra with a gray cloud deck at 0.1 bar for reference, which is the position of the top of the troposphere.

Note that we do not include stars later than K or earlier than G, as they are not our primary targets. Actually, planets around stars with spectral type later than K have much higher signals than those around GK stars, which means that any configuration that can detect spectral signals from Earth-like planets around a K star can detect those Earth-like planets around M and less massive stars assuming the planets are outside of the inner working angle (IWA). The IWA is the smallest angular separation between a host and companion source at which the faint companion is detectable. On the other hand, Earth-like planets around F-type stars have too small contrast ratios for solid detection even by a 6 m space telescope with the fancy parameters.

For reflection spectra, surface albedo is set to 0.3 and phase angle to 45°. For simplicity, we assume all the planets in consideration are beyond the IWAs of our proposed coronagraph, which is ∼25 and 46 mas for the UV and VIS bands respectively. The latter value corresponds to a conservative middle HZ radius of G0 and K9 stars ∼40 and 20 pc away, respectively.

Figure 3 features as examples the reflection and transmission spectra with or without water clouds of a twin Earth at a 1 au orbit of a G2 star at three different R. For the reflection spectra,

those in yellow include the contribution from starlight leakage with a suppression level of 10^{-10} for comparison. In each of the right panels, the yellow transmission spectrum illustrates the case of a twin Earth atmosphere with a gray cloud deck present at 0.1 bar, i.e., the atmosphere below this deck cannot be probed due to either a large absorption opacity or atmospheric diffraction.

3.2. Simulated Spectra

An observed planet reflection spectrum $F_{\rm p}^{\rm R,Obs}(\lambda)$ is simply the addition of a planet spectrum, a stellar spectrum that was not blocked from a stellar light suppression instrument and noise, while a transmission planet spectrum $F_{\rm p}^{\rm T,Obs}(\lambda)$ consists of a model planet spectrum and noise, assuming the stellar contribution has been removed clearly by contrasting the in-transit spectrum with the out-of-transit spectrum. The leakage stellar signal is estimated by simply multiplying the stellar spectrum by the starlight suppression level C.

As described in Section 3.1, a model planet spectrum is generated by petitRADTRANS, while a synthetic stellar spectrum $F_{*}^{\rm Mod}(\lambda)$ is obtained from the PHOENIX library (Husser et al. 2013). Both spectra are then convolved with a Gaussian profile that corresponds to a certain spectral resolution R. Then Poisson noise is added to the convolved spectrum assuming a Gaussian distribution, with a certain S/N at the reference wavelength at 0.88 μm and any other wavelength of interest, (see definition of S/N and S/N(λ) in Section 3.4). In the top panels of Figure 3, the simulated observation spectra with S/N = 20 for reflection spectra and S/N = 1000 for transmission spectra from 0.8 to 1.05 μm are overplotted with error bars as examples.

Although Tianlin is proposed to cover a wavelength range of 0.2–1.7 μm, here in this work we use only the 0.8–1.0 μm part for the simulation. The main purpose of this simulation is to verify whether a water feature can be detected in a specific star-planet system and what is the required integration time. Although water has strong features in NIR, the currently available NIR detectors that may be employed for Chinese missions can probably suffer from large readout noise and dark current, making it more difficult to detect water features in NIR than in optical. In optical, the strongest water features reside in the 0.8–1.0 μm range, thus including other bands will not enhance signals significantly. On the other hand, enlarging wavelength coverage will require much more time for the spectral information retrievals, particularly for high-R cases. Detailed simulation with wider spectral coverage and on other species will be performed in the future.

In summary, the observed reflection and transmission spectra are given respectively by:

$$F_{\rm p}^{\rm R,Obs}(\lambda) = F_{\rm p}^{\rm R,Mod}(\lambda) + F_{*}^{\rm Mod}(\lambda)\cdot C + P(\lambda), \quad (2)$$

and

$$F_{\rm p}^{\rm T,Obs}(\lambda) = F_{\rm p}^{\rm T,Mod}(\lambda) + P(\lambda), \quad (3)$$

where $P(\lambda)$ is the added Poisson noise, at a given S/N.

3.3. Molecular Constraint Definition

The key to this simulation is to detect H_2O in a simulated observation, thus its mixing ratio is of primary interest. Following the same method of analyzing real observed planet spectra, a spectral retrieval technique is employed to infer the temperature structure and chemical compositions of the target planet from the observed spectra. We define a *constraint* if a posterior shows a localized peak and has a 1σ range of less than 1/5 for retrieved posterior values. For H_2O in our simulation, the input of the mixing ratio is -3.2 in logarithmic scale, and thus the 1σ range is less than 0.6 orders of magnitude. Our criteria for a constraint are thus stronger than those defined in Feng et al. (2018) and Smith et al. (2020), in which a one order of magnitude 1σ range will define a constraint.

The mixing ratio of a certain molecule is thus retrieved using the Nested Sampling Monte Carlo package PyMultiNest (Buchner et al. 2014) of petitRADTRANS from the simulated spectra with a certain S/N and spectral resolution R. In this way, the lowest S/N values to achieve a constraint on H_2O VMR are then determined for each spectrum at a given R.

3.4. S/N and Total Integration Time

We use the noise model of Robinson et al. (2016) for the estimation of S/N that could be achieved by a given instrument. The desired S/N values at a certain λ are connected to total integration times $t_{\rm int}$ for a set of technical parameters and a given noise model. Following Equation (6) in Robinson et al. (2016), assuming background subtraction will be performed to detect the planet signal, the total integration time $t_{\rm int}$ required for a reflection spectrum to reach a given S/N is related to the background count rate and planet photon count rate, i.e.,

$$t_{\rm int} = \frac{n_{\rm p} + 2n_{\rm b}}{n_{\rm p}^2}{\rm S/N}^2, \quad (4)$$

where $n_{\rm p}$ is the planet photon count rate, $n_{\rm b} = n_{\rm z} + n_{\rm ez} + n_{\rm lk} + n_{\rm D} + n_{\rm R}$ is the total background count rate, $n_{\rm z}$ is local zodiacal light count rate, $n_{\rm ez}$ is exozodiacal light count rate, $n_{\rm lk}$ is the leakage starlight photon count rate from the coronagraph and $n_{\rm D}$ is dark noise rate. As our observation shall normally stare at one target for long exposures, the detector readout noise rate is significantly smaller than the other noise and thus is not taken into account in this study. The zodiacal and exozodiacal background count rates are given using Equations (8) and (9) and the quoted V band surface brightness in Stark et al. (2019). More detailed calculations of each source of noise can be found in Robinson et al. (2016). For example, for the case of an

Earth-twin around a $V=5$ Sun-like star, when $C=10^{-9}$, $\eta=0.1$ and $D=6$ m, we have $n_{\rm p}=2.85\times10^{-3}$ s^{-1}, $n_{\rm z}=5.66\times10^{-2}$ s^{-1}, $n_{\rm ez}=1.42\times10^{-1}$ and $n_{\rm lk}=7.38\times10^{-3}$ s^{-1}, then $n_{\rm b}=0.21$ s^{-1}. If we require an S/N of 19.8, we need a $t_{\rm int}=5.64\times10^{3}$ hr. The corresponding S/N$_{\rm mol}$ (as described below) for water is 3.

For transmission spectra, as photon noise from host stars vastly dominates background noises, S/N can be accurately estimated by $n_{\rm p}/n_{*}^{0.5}$, where $n_{*}=\eta F_{*}t_{\rm int}$ and $n_{\rm p}=\eta F_{*}t_{\rm int}\Delta(R_{\rm p}/R_{*})^2$. Thus we have

$$t_{\rm int} = \frac{\rm S/N^2}{\eta F_{*}\Delta(R_{\rm p}/R_{*})^2}, \quad (5)$$

where $\Delta(R_{\rm p}/R_{*})^2$ stands for the transmission spectral signal of the tracing molecule. Note that currently we use a wavelength-independent end-to-end throughput η for our simulation.

It is obvious that the S/N is λ-dependent. We set the reference point of S/N at $\lambda=0.88$ μm, just outside of the water band. Considering the integration time is constant in a single bandpass, S/N(λ) can be derived using the following two equations for reflection and transmission spectra

$$\rm S/N(\lambda)^2\frac{n_p(\lambda)+2n_b(\lambda)}{n_p(\lambda)^2}=S/N(\lambda_0)^2\frac{n_p(\lambda_0)+2n_b(\lambda_0)}{n_p(\lambda_0)^2}, \quad (6)$$

and

$$\rm S/N(\lambda)^2\frac{n_*(\lambda)}{n_p(\lambda)^2}=S/N(\lambda_0)^2\frac{n_*(\lambda_0)}{n_p(\lambda_0)^2}. \quad (7)$$

Note that the total integration time required to achieve a given S/N is different from the S/N$_{\rm mol}$, which is the minimum S/N required to detect a certain molecule as defined for example by Brandt & Spiegel (2014). The main difference between S/N and S/N$_{\rm mol}$ is the definition of the signal. The signal involved in S/N$_{\rm mol}$ is the molecular spectral feature imprinted on the continuum, i.e., the difference between the continuum level and the valley value (or the peak value) for the case of an emission (or transmission) spectrum. For a given planet spectrum, the two S/Ns are numerically connected. Taking the $R=150$ clear emission spectrum as an example (the blue curve in the top-left of Figure 3), the signal component of S/N is $F_{\rm p}/F_{\star}$ and equals $\sim4\times10^{-10}$ at 0.88 μm, while the signal part of S/N$_{\rm mol}$ for H_2O is $F_{\rm p}/F_{\star}(0.88\,\mu{\rm m})-F_{\rm p}/F_{\star}(0.94\,\mu{\rm m})\approx4\times10^{-10}$–$2\times10^{-10}=2\times10^{-10}$. So, for this case, the S/N at 0.88 μm is about twice the S/N$_{\rm H_2O}$. Based on this noise-free spectrum, we generate a series of noisy spectra with different S/N$_{\rm H_2O}$, which are used to determine the abundance of H_2O via the retrieval analysis. The smallest S/N$_{\rm H_2O}$ that allows a "constraint" on H_2O abundance is the S/N$_{\rm mol}$, and the S/N(0.88 μm) can be calculated from the corresponding noisy spectra. The last step is to calculate $T_{\rm int}$ using Equation (4).

4. Results and Discussion

4.1. Direct Spectroscopy

Our simulation suggests that under the optimized instrumental performance, Tianlin is expected to yield emergent spectra with S/N$_{\rm mol}=5$ for H_2O with its coronagraph after integrating 10^2–10^3 hr for the vast majority of standard and wet Earth-like planets in the HZs of G8-K7 stars, assuming a phase angle of 90°. Increasing D to 6 m will make Tianlin capable of measuring the water vapor of a nearby twin Earth in less than 10^3 hr.

The main results of our simulation on reflection spectra are presented in Figure 4, which shows the dependence of $t_{\rm int}$ on D, C and η for a twin Earth with Earth-like water vapor content. The dependence on dark current rate d is very weak until d exceeds 2e$^-$/h/pixel, and even lower dark current has already been accomplished by modern detectors developed by companies such as Teledyne e2v.[8] This is reasonable because in this regime, noise is dominated by local zodiacal and exozodiacal light backgrounds.

It is clear from Figure 4 that $t_{\rm int}$ is very sensitive to C, the contrast of a coronagraph or an external starshade, especially when $C>10^{-9.5}$. It must be better than 10^{-9} to constrain H_2O of a twin Earth in a maximum affordable integration time, i.e., less than 10^4 hr, or about 1 yr. Therefore, the starlight suppression performance, particularly the contrast C, is critical for the achievement of Tianlin's objective. Such limits can be achieved in a laboratory experiment with a raw contrast of 10^{-9} or better at visible wavelengths (Trauger & Traub 2007; Dou & Ren 2016; Mejia Prada et al. 2019; Llop-Sayson et al. 2020; Harness et al. 2021), and the improved post-processing analysis could further reduce residual starlight speckles. It will be certainly more challenging to realize such a high contrast on board a spacecraft, mainly due to fast line-of-sight jitter and slow wave front drift. As shown in Gaudi et al. (2020), the self-induced pointing jitter for a HabEx-like telescope at the L2 point with tiny thermal and gravitational gradient disturbances should be nonexistent, but the reaction wheels or microthrusters may induce pointing jitter on the order of $10^{-4}''$ rms. The simulation done for HabEx shows that such jitter will not affect the raw contrast at IWA to the level of 3×10^{-10}. On board testing in space for $>10^8$ starlight suppression will be carried out on the near-future RST (Akeson et al. 2019), and $\sim10^8$ contrast ratio on the Chinese Space Station Telescope (see, CSST whitebook, private communication).

In addition, Figure 4 suggests that the second key technical parameter D should not be smaller than 6 m. It requires more than 1550 and 670 hr for $D=4$ m or 6 m respectively, assuming $C=10^{-10}$ and $\eta=0.1$. These two numbers increase dramatically to 13,000 and 5600 hr for $C=10^{-9}$. Therefore, a primary mirror with $D=4$ m seems not large enough to secure

[8] https://www.teledyne-e2v.com/

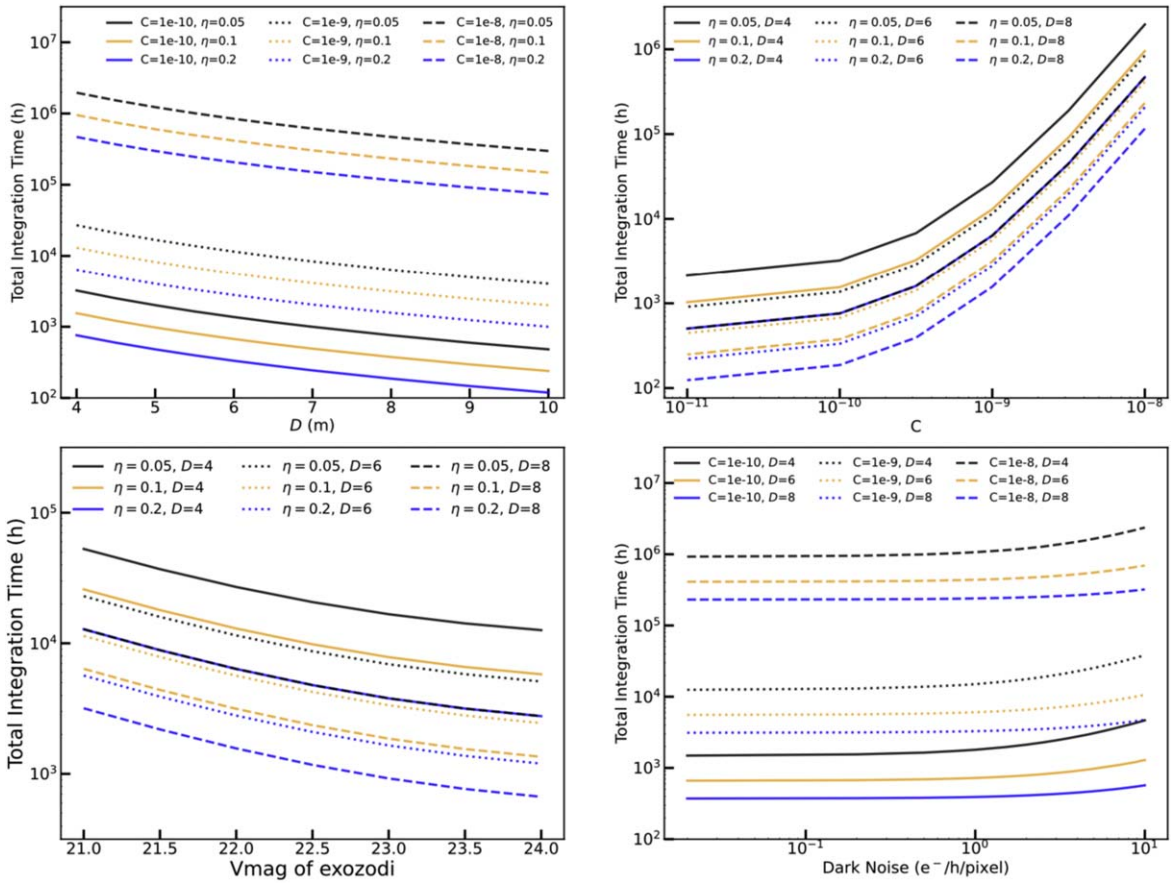

Figure 4. Left: The dependence of total integration time $t_{\rm int}$ on aperture size D for the direct spectroscopy technique. $t_{\rm int}$ is the minimum integration time for a constraint of water vapor on a twin Earth around a $V = 5$ G2V star, based on our simulation of $R = 150$ reflection planet spectra. Lines with different styles and colors represent different $t_{\rm int}$–D dependence with different C and η. Right: The dependence of $t_{\rm int}$ on C with different combinations of η and D.

robust detection of atmospheric biosignatures from Earth-like planets, especially in cases where the planet is smaller than Earth, or the star is larger and brighter than the Sun, or the planetary system is more than 10 pc from us. Enlarging D to 6 m will result in a gain in photons by a factor of $\sim$2, which will consequently largely increase the number of planets that can be observed and characterized. It is also shown that the higher η is, the shorter $t_{\rm int}$ that is required. Increasing η seems to have a similar effect as increasing D, because both parameters are directly related to the number of photons received.

4.2. Transmission Spectroscopy

On the other hand, our results show that when relying on classic low resolution ($R \sim 150$) transit spectroscopy, much longer $T_{\rm int}$ is required to achieve the same $S/N_{\rm mol}$. For example, as affirmed by the starting points of the lines in Figure 5, a 6 m telescope needs to integrate $\sim$50 and $>$180 hr to constrain H_2O VMR at 0.94 μm for an Earth-sized planet orbiting a K7 and K2-G2 dwarf star $\sim$10 pc away, respectively. Unfortunately, for transit spectroscopy, the total usable integration time is strictly limited by the number of transits that could be covered in the mission's lifetime and the duration of each transit, with the latter being about 13 hr for the Sun–Earth system. For Tianlin, a conservative mission lifetime is 5 yr, with possible 5 yr extension. Therefore, the total integration time is approximately 65 and 130 hr, for a habitable planet around a G2 and K7 star, respectively. Increasing D to 8 m will significantly shorten the required $T_{\rm int}$, and thus make it possible to detect H_2O with $S/N \sim 5$ on an Earth-like planet in the HZ of a K type star in the mission lifetime, however for the same case around G types stars, one may need $D \geqslant 8$ m to detect H_2O.

Lastly, we have studied the advantages of using a high-R technique for transit spectroscopy. Our simulations show that increasing R will significantly shorten the required $T_{\rm int}$ time, at least for nearby bright stars. As demonstrated in Figure 5, for a constraint on water content on an Earth-like planet around a G2 star at 10 pc, Tianlin with D of 6 m demands $T_{\rm int} \sim 380$, 600 and 210 hr with $R = 150$, 1500 and 15,000, respectively.

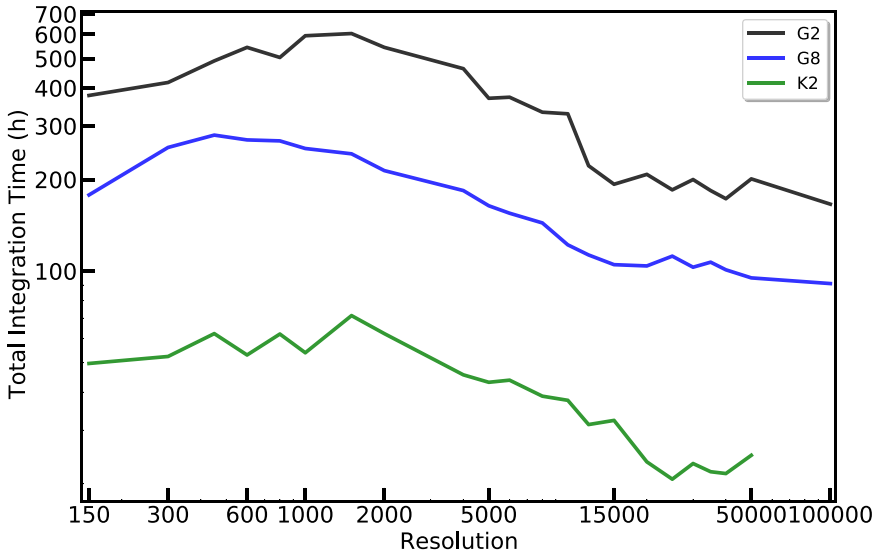

Figure 5. The required total integration time for a 6 m space telescope to obtain a constraint on the water feature at 0.94 μm varying with spectral resolution R for an Earth-like planet orbiting a dwarf star of $V = 5$ with a spectral type of G2, G8 or K2, assuming the noise follows a Gaussian distribution. Note that this is the total integration time during primary transits, which is ∼13 hr per year for a Sun–Earth system, and is ∼65 hr for a 5 yr mission lifetime.

Increasing R will lead to two contrary changes of S/N and thus $t_{\rm int}$. On one hand, the molecular signal per pixel decreases linearly with increasing R, while the detector noise does not change, and thus the S/N will decrease proportionally to approximately the square root of R. On the other hand, when R increases, the total integrated signal of many individual lines of a molecule will first increase quickly because the mixed individual lines at low R will gradually separate from each other, and the peak intensity of each line will increase as well. Nevertheless, the increase will turn slow and eventually stop after all individual lines are separated and the instrumental lines' width becomes smaller than the intrinsic widths of planet lines. The combination of these two effects results in a decrease and then an increase of $t_{\rm int}$ when R changes from ∼100 to ∼1000, followed by a steady decrease to $R \sim 15{,}000$ for a G2 and G8 host star, and to $R \sim 20{,}000$ for K2 host stars. This trend is reasonable given that the median separation of every two adjacent water lines in the wavelength range from 0.8 to 1.05 μm is found to be 0.6 Å, corresponding to a resolution of ∼13,000–16,000. Specifically, when $R = 150$, only 0.07% of lines could be separated well from their neighbors and thus resolved. This fraction only increases to 1.9% for $R = 1000$, and is 53% and 61% for $R = 15{,}000$ and 20,000, respectively.

We point out one important bonus advantage for the case of $R > 15{,}000$ which has not been taken into account in the above analysis. The molecular signals from individual lines can be combined by cross-correlating the observed spectra with a model template spectrum. In this way, the significance of a molecular species is subsequently enhanced by the square root of $N_{\rm lines}$, which is a multiplication factor that takes into account the number and strength of the individual planet lines involved (Snellen et al. 2015). For the 0.94 μm H_2O band, we find that $N_{\rm lines} \geqslant 100$. Therefore, the required $T_{\rm int}$ in theory for a twin Earth should be less than 100 hr using the cross-correlating technique. Simulation will be performed in the future to confirm this number.

The high-resolution spectroscopy can be also used in conjunction with the high contrast imaging technique as well to achieve a contrast ratio of 10^{-10} in ideal cases (Snellen et al. 2015; Wang et al. 2018). A more realistic simulation will be further performed in order to identify the R value which is the best for detecting molecular signals, and in the meanwhile can be realized in a space telescope at reasonable expense.

5. Summary

To summarize, the Tianlin mission is a space telescope with a 6+ meter aperture proposed in China with the primary objective to detect biosignatures of Earth-like planets in the HZs of nearby GK dwarf stars. Its design will be optimized for high-contrast imaging aided by an advanced coronagraph and medium-to-high resolution spectroscopy with a light, compact and stable spectrograph. In addition, Tianlin may yield a comprehensive understanding of the characteristics, formation and evolution of planets by conducting a complete survey of gas giant planets to rocky planets orbiting nearby stars. Moreover, Tianlin will provide tremendously higher quality data for the studies of almost all astrophysical fields, including cosmology, galaxies, stars and interstellar medium, and should largely enhance our understanding of the universe and its contents.

A preliminary concept study has been conducted in order to yield the optimal and tolerable values for a set of key technical parameters for the telescope and its instrumentation. The study is based on a set of simulated planet spectra generated using petitRADTRANS, taking into consideration various stellar and planet parameters and a range of technical parameters. We conclude that to achieve our primary science goal, D is recommended to be no less than 6 m, C should be better than 10^{-9} and $\eta_{\rm cor}$ larger than 0.1, assuming a classic internal coronagraph rather than an external starshade will be deployed. We find that the current λ range is good enough for our purpose, and will explore other λ ranges for smaller $t_{\rm int}$. We point out that increasing spectral resolution to ~15,000–20,000 may largely improve the detection capability of molecular signals with transmission spectra, similar to the case of reflection spectra, in the sense that combining high spectral resolution with high contrast imaging could significantly enhance the capability of detecting tiny signals. Extending wavelength coverage to 0.20 μm, or even shorter, will not only allow the detection of biosignature O_3, but also enable great developments in various studies including the cosmic web, high-energy physics in stars and galaxies, for which extreme-UV (EUV) is the best window, but which however has been ignored for now and in the coming decades. Additional in-depth and more realistic simulations are ongoing to further constrain and better refine the baseline configuration of Tianlin, which will be followed by a feasibility study in the coming years.

Acknowledgments

This research is supported by the National Natural Science Foundation of China (NSFC, grants Nos. 62127901, 11988101, 42075123 and 42005098), the National Key R&D Program of China No. 2019YFA0405102, and the Strategic Priority Research Program of Chinese Academy of Sciences (CAS), grant Nos. XDA15016200 and XDA15072113. M. Z. is supported by the Chinese Academy of Sciences (CAS), through a grant to the CAS South America Center for Astronomy (CASSACA) in Santiago, Chile. We acknowledge the science research grants from the China Manned Space Project with No. CMS-CSST-2021-B12.

ORCID iDs

Wei Wang https://orcid.org/0000-0002-9702-4441
Meng Zhai https://orcid.org/0000-0003-1207-3787
Gang Zhao https://orcid.org/0000-0002-8980-945X

References

Akeson, R., Armus, L., Bachelet, E., et al. 2019, arXiv:1902.05569
Barclay, T., Pepper, J., & Quintana, E. V. 2018, ApJS, 239, 2
Benneke, B., Wong, I., Piaulet, C., et al. 2019, ApJL, 887, L14
Borucki, W. J., Koch, D. G., Basri, G., et al. 2011, ApJ, 728, 117
Brandt, T. D., & Spiegel, D. S. 2014, PNAS, 111, 13278
Buchner, J., Georgakakis, A., Nandra, K., et al. 2014, A&A, 564, A125
Des Marais, D. J., Harwit, M. O., Jucks, K. W., et al. 2002, AsBio, 2, 153
Dou, J., & Ren, D. 2016, ApJ, 832, 84
Feng, Y. K., Robinson, T. D., Fortney, J. J., et al. 2018, AJ, 155, 200
Gardner, J. P., Mather, J. C., Clampin, M., et al. 2006, SSRv, 123, 485
Gaudi, B. S., Seager, S., Mennesson, B., et al. 2020, arXiv:2001.06683
Ge, J., Zhang, H., Zang, W., et al. 2022, arXiv:2206.06693
Harness, A., Shaklan, S., Willems, P., et al. 2021, JATIS, 7, 021207
Howell, S. B., Sobeck, C., Haas, M., et al. 2014, PASP, 126, 398
Husser, T. O., Wende-von Berg, S., Dreizler, S., et al. 2013, A&A, 553, A6
Ji, J.-H., Li, H.-T., Zhang, J.-B., et al. 2022, RAA, 22, 072003
Kasdin, N. J., Bailey, V. P., Mennesson, B., et al. 2020, Proc. SPIE, 11443, 114431U
Kiang, N. Y., Domagal-Goldman, S., Parenteau, M. N., et al. 2018, AsBio, 18, 619
Kopparapu, R. K., Ramirez, R. M., SchottelKotte, J., et al. 2014, ApJL, 787, L29
Léger, A., Defrère, D., García Muñoz, A., et al. 2019, AsBio, 19, 797
Llop-Sayson, J., Ruane, G., Mawet, D., et al. 2020, AJ, 159, 79
Mayor, M., & Queloz, D. 1995, Natur, 378, 355
Mejia Prada, C., Serabyn, E., & Shi, F. 2019, Proc. SPIE, 11117, 1111709
Mollière, P., Wardenier, J. P., van Boekel, R., et al. 2019, A&A, 627, A67
Rauer, H., Catala, C., Aerts, C., et al. 2014, ExA, 38, 249
Ricker, G. R., Winn, J. N., Vanderspek, R., et al. 2015, JATIS, 1, 014003
Robinson, T. D., Stapelfeldt, K. R., & Marley, M. S. 2016, PASP, 128, 025003
Smith, A. J. R. W., Feng, Y. K., Fortney, J. J., et al. 2020, AJ, 159, 36
Snellen, I., de Kok, R., Birkby, J. L., et al. 2015, A&A, 576, A59
Snellen, I. A. G., Brandl, B. R., de Kok, R. J., et al. 2014, Natur, 509, 63
Stark, C. C., Belikov, R., Bolcar, M. R., et al. 2019, JATIS, 5, 024009
Swain, M. R., Estrela, R., Roudier, G. M., et al. 2021, AJ, 161, 213
The LUVOIR Team 2019, arXiv:1912.06219
Tinetti, G., Drossart, P., Eccleston, P., et al. 2016, Proc. SPIE, 9904, 99041X
Trauger, J. T., & Traub, W. A. 2007, Natur, 446, 771
Wang, J., Mawet, D., Hu, R., et al. 2018, JATIS, 4, 035001
Wang, J., Mawet, D., Ruane, G., Hu, R., & Benneke, B. 2017, AJ, 153, 183
Wang, W., Zhai, M., Zhao, G., et al. 2020, Proc. SPIE, 11443, 114431Z